Tradeoffs in imager design parameters for sensor reliability

Glenn H. Chapman[*a], Jenny Leung[a], Rahul Thomas[a], Zahava Koren[b], Israel Koren[b]

[a]School of Engineering Science, Simon Fraser University, 8888 University Drive, Burnaby, BC, Canada, V5A 1S6
[b]Dept. of Electrical & Computer Engineering, Univ. of Massachusetts, Amherst, MA, USA 01003

ABSTRACT

Image sensors are continuously subject to the development of in-field permanent defects in the form of hot pixels. Based on measurements of defect rates in 23 DSLRs, 4 point and shoot cameras, and 11 cell phone cameras, we show in this paper that the rate of these defects depends on the technology (APS or CCD) and on design parameters the like of imager area, pixel size, and gain (ISO). Increasing the image sensitivity (ISO) (from 400 up to 25,600 ISO range) causes the defects to be more noticeable, with some going into saturation, and at the same time increases the defect rate. Partially stuck hot pixels, which have an offset independent of exposure time, make up more than 40% of the defects and are particularly affected by ISO changes. Comparing different sensor sizes has shown that if the pixel size is nearly constant, the defect rate scales with sensor area. Plotting imager defect/year/sq mm with different pixel sizes (from 7.5 to 1.5 microns) and fitting the result shows that defect rates grow rapidly as pixel size shrinks, with an empirical power law of the pixel size to the -2.5. These defect rate trends result in interesting tradeoffs in imager design.

Keywords: defect detection, hot pixel, imager defects, active pixel sensor, APS, CMOS image sensor, demosaicing

1. INTRODUCTION

Digital imager technology now dominates the photographic field and is becoming very common in embedded sensor design. Just like any other microelectronic device, digital imager sensors develop defects over time. However, unlike other digital devices, most in-field defects in digital imagers begin appearing soon after fabrication, are permanent and their number increases continuously over the lifetime of the sensor. These faulty pixels degrade the quality of the image captured by the sensor. Although the impact of defects can be overcome by factory calibration, this can be expensive for the users and is often infeasible for imagers used in remote sensing applications.

Through on-going investigations of imager in-field defect development we have identified the characteristics and rate of faulty pixels [1-6], and pinpointed the in-field defect causal mechanism, thus helping in the development of a better defect correction method [2,6]. In this study we have added data from cameras with small pixels, and a range of sensor areas. We now have collected enough data to identify important differences in defect development rates that are related to several imager parameters: in particular, the area of the imager array, the pixel cell size, the pixel type (CCD or CMOS), and sensor gain (ISO). We present in this paper the important trends in imager defect development. First, for the common defect type of hot pixels, we show how sensor gain (ISO) significantly affects the number and appearance of defects in the images, including the creation of full stuck high pixels. Then, we show how the temporal growth rate changes with ISO. Next, we explore how the area of the imager affects defect rates. Finally, we show how scaling down the pixel cell size results in a rise in the number and strength of the defects, and establish an empirical relationship between the defect rate and the pixel size.

[*] glennc@cs.sfu.ca; phone 1-778-782-3814; fax 1-778-782-4951; http://www.ensc.sfu.ca/people/faculty/chapman/; School of Engineering Science, Simon Fraser University, 8888 University Drive, Burnaby, BC V5A 1S6, Canada

Sensors, Cameras, and Systems for Industrial, Scientific, and Consumer Applications XII, edited by Ralf Widenhorn, Valérie Nguyen, Proc. of SPIE-IS&T Electronic Imaging, SPIE Vol. 7875, 78750I · © 2011 SPIE-IS&T · CCC code: 0277-786X/11/$18 · doi: 10.1117/12.876947

2. HOT PIXEL

In our previous study [5,6], we have performed manual calibrations on numerous commercial DSLRs. In particular, we used dark field exposure (i.e., no illumination) to test for stuck-high and partially stuck defects, and bright field (i.e., uniform illumination at near saturation) to test for stuck-low defects. However, in our experiments, we have not found any of these stuck defect types. Instead, hot pixels were the dominating defect type. A hot pixel has an illumination-independent component that increases linearly with exposure time, and can, therefore, be identified by capturing a series of dark field images at increasing exposure times. The dark response of a hot pixel is demonstrated in Figure 1 showing the normalized pixel illumination vs. exposure time (illumination level 0 represents no illumination and 1 represents saturation). The dark response of a good pixel should be close to 0 (with some variation due to noise in the sensor) at any exposure level, as shown in plot 1(a). In addition, we have found [5] that hot pixels can be categorized into two types: standard hot pixels, as shown in plot 1(b), which have an illumination-independent component that increases linearly with exposure time; and partially stuck hot pixels, as shown in plot 1(c), which have an additional offset that can be observed at no exposure.

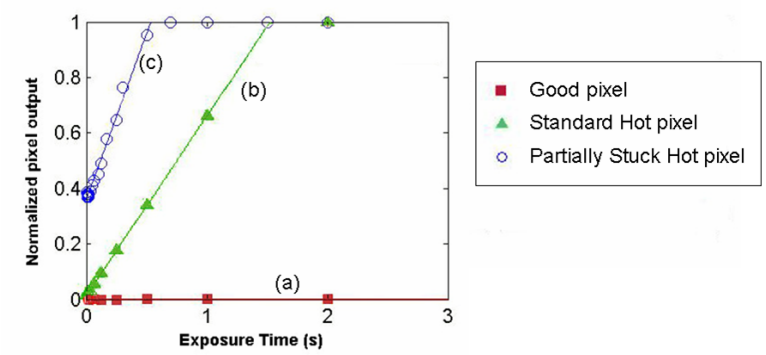

Figure 1: Comparing the dark response of a good pixel and a hot pixel.

A typical operation of a pixel can be modeled using Equation (1), where R_{photo} measures the incident illumination rate, R_{Dark} is the dark current rate, T_{exp} measures of the exposure setting, b is the dark offset, and m is the amplification from the ISO setting, which is directly proportional to the ISO level.

$$I_{Pixel}(R_{photo}, R_{Dark}, T_{\exp}, b) = m \cdot (R_{photo} T_{\exp} + R_{Dark} T_{\exp} + b) \quad (1)$$

In the case of a good pixel, both R_{Dark} and b are zero; therefore, the output from such a pixel is simply the measure of incident illumination. For a hot pixel, two more terms are added on top of the incident illumination; thus the output from such a pixel will appear brighter. The dark response of a pixel can be estimated by setting R_{photo} = 0, and Equation (1) is then simplified into

$$I_{offset}(R_{Dark}, T_{\exp}, b) = m \cdot (R_{Dark} T_{\exp} + b) \quad (2)$$

Based on Equation (2), the calculation of the dark response, also called the combined dark offset, of any hot pixel resembles a linear equation. By plotting the pixel dark response vs. exposure time, as shown in Figure 1, a linear function can be used to estimate R_{Dark} and b. For a standard hot pixel b is zero, and therefore, this type of defects is most visible in long exposure images. For partially stuck hot pixels, on the other hand, the response depends on the magnitude of b and this type of defects will appear in all images.

In our long duration study we have identified hot pixels from 21 DSLR cameras including both APS and CCD sensors, with the age of these cameras varying between 1 and 6 years (Table 1). After performing the dark-frame calibration at ISO 400, our results show a cumulative total of 243 hot pixels of which 44% are of the partially stuck type. The offset in partially stuck hot pixels causes this type of defects to appear at any exposure level, which therefore has a greater impact on the image quality.

2.1 Impact of ISO on hot pixels

ISO setting is one of the most common functions used among photographers. It provides amplification of the pixel output, thus an object can still be captured even under low light conditions. The amplification level scales

proportionally with the ISO setting, but the usable ISO range is limited by the noise level of the sensor. Before 2004, most commercial DSLRs had a usable ISO range of 100 to 1600. As sensor technology improved, noise levels have been reduced and the usable ISO range has expanded. Some of the new DSLR models sold today have a usable ISO range of up to 25600. The ability to capture images at high ISO is a great benefit to photographers as it permits natural light photography without the need for flash or a long exposure setting.

Table 1: Summary of in-field defects from tested cameras at ISO 400.

Camera	Sensor Type	# of pixels (MP)	Sensor size (mm)	Pixel size (μm)	Total Age (years)	Hot Pixels		
						Standard	Partially stuck	Total
A	APS	6.3	22.7 × 15.1	7.38 × 7.36	6	0	12	12
B	APS	21.0	36.0 × 24.0	6.26 × 6.26	1	0	7	7
C	APS	6.3	22.7 × 15.1	7.38 × 7.36	4	1	5	6
D	APS	12.2	22.2 × 14.8	5.14 × 5.14	2	1	1	2
E	APS	8.0	22.2 × 14.8	6.33 × 6.33	2	0	1	1
F	APS	12.2	22.2 × 14.8	5.14 × 5.14	0.8	0	3	3
G	APS	21.0	36.0 × 24.0	6.26 × 6.96	0.5	0	1	1
H	APS	8.2	22.5 × 15.0	6.30 × 6.30	4	1	3	4
I	APS	10.1	22.2 × 14.8	5.59 × 5.59	1	0	1	1
J	CCD	6.0	23.7 × 15.5	7.96 × 7.57	4	17	0	17
K	CCD	10.0	23.6 × 15.8	5.87 × 5.87	5	6	16	22
L	CCD	10.0	23.6 × 15.8	5.87 × 5.87	5	11	23	34
M	CCD	10.0	23.6 × 15.8	5.87 × 5.87	5	12	16	28
N	CCD	10.0	23.6 × 15.8	5.87 × 5.87	2	17	1	18
O	CCD	6.0	23.7 × 15.5	7.69 × 7.57	NA	0	7	7
P	CCD	6.0	23.7 × 15.5	7.69 × 7.57	2.5	9	1	10
Q	APS	8.2	22.5 × 15.0	6.30 × 6.30	2	0	2	2
R	CCD	6.0	23.7 × 15.5	7.69 × 7.57	2.5	17	0	17
S	CCD	10.0	23.6 × 15.8	6.10 × 6.10	0.5	5	6	11
T	APS	12.2	23.7 × 15.7	5.39 × 5.38	2	0	0	0
U	CCD	5.3	23.7 × 15.5	7.87 × 7.90	5	26	0	26
Total						**137**	**106**	**243**

In our previous analysis we have performed all calibrations at ISO 400 as the noise level at this setting is very small in most cameras. However, observing Equation (1), the numerical gain that is applied to the pixel output amplifies the defect parameters as well. To observe the impact of ISO on defective pixels, we have performed the dark frame calibration at different ISO levels. Due to the increase in the background noise at higher ISO, the threshold value used to identify defects was adjusted [6]. Table 2 summarizes the results of out most recent calibration on a set of 13 DSLR cameras at varying ISO settings. As seen in Table 2, the number of identified defects increased as the ISO amplification increased. At ISO 400 we accumulated a total of 137 defects, and this almost doubled to 240 defects at ISO 800. At ISO 1600 we had a total of 367 defects, which is 2.7 times higher than the defects at ISO 400. This shows that at low ISO, many of the defects cannot be distinguished from noise signals but they appear when the ISO is increased. By calibrating at higher ISO, defect parameters are being amplified as in Equation (2) and the distinction between noise and defect become clearer.

In Figure 2 we compare the dark response of an identified hot pixel at varying ISO levels. It is clear that at ISO 400, the defect has low values of R_{Dark} and b; as the ISO amplification increases, both R_{Dark} and b increase dramatically. In fact, at ISO 12800 the dynamic range of the pixel is reduced by 40% solely due to the offset b, and at ISO 25600, the pixel is near saturation at all exposures. Given the high number of hot pixels with offsets suggests that the development of stuck high pixels in the field may actually be due to the presence of hot pixels with very high offsets. This is consistent with our experience of never detecting a true stuck pixel in our cameras, but noting that there is mention of a few cameras developing stuck pixels in camera forums.

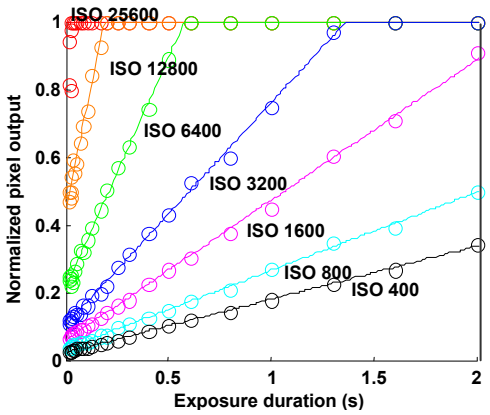

Figure 2: Dark response of a hot pixel at various ISO levels.

Table 2: Summary of defect count at various ISO levels.

Camera	Age	ISO				
		100	200	400	800	1600
A	6	4	11	12	23	25
B	1	1	4	7	15	22
C	4	0	1	6	11	19
D	2	1	1	2	4	10
E	2	0	0	1	5	12
F	0.8	1	1	2	3	6
G	0.5	0	0	1	1	2
H	4	0	0	4	7	12
I	1	0	0	1	5	8
J	4	0	10	17	23	33
K	5	8	15	22	43	69
L	5	11	17	34	52	67
M	5	11	18	28	48	82
Cumulative Total:		**37**	**78**	**137**	**240**	**367**

With the amplification from ISO, the I_{Offset} as calculated by Equation (2) dominates the illumination signal, causing further reduction in the pixel dynamic range. To see how the defect parameters vary over different ISO levels, we have plotted a histogram of I_{Offset} calculated at a common exposure of 0.5s (Figure 3(a)) and a long exposure of 1s (Figure 3(b)). In Figure 3(a) we can see that at 0.5s, most of the defects are low impact defects and have an I_{Offset} value below 0.1, but at ISO 400 about 10% of the defects will have an I_{Offset} of 0.2. With an ISO of 1600, about 10% of the identified defects will saturate even at 0.5s. Looking at a longer exposure of 1s, as in Figure 3(b), we can see that the majority still has I_{Offset} below 0.1, but at the same time the number of pixels with I_{Offset} over 0.2 has increased by 20%. In fact, at ISO 1600, about 20% of the defects are at saturation. Pixels with an I_{Offset} of 0.2 will reduce their dynamic range by 20%. The important point here is that at high ISO settings there are considerably more observed hot pixels and they affect a wider range of exposure times.

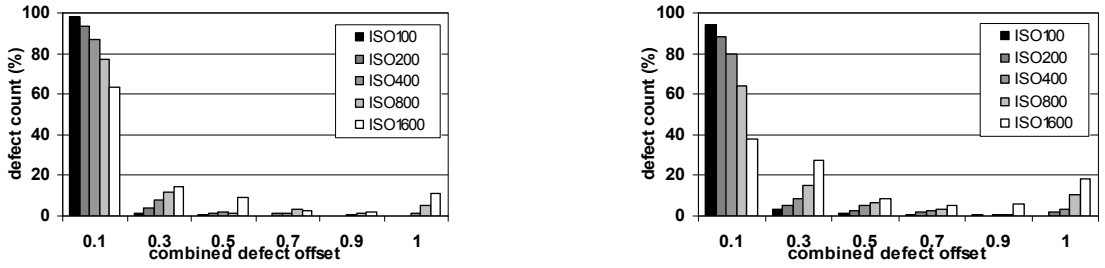

(a) 1/2s **(b) 1s**

Figure 3: Histogram of I_{offset} at varying ISO levels and two exposure times.

3. SPATIAL AND TEMPORAL DEFECT ANALYSIS

In our previous study, we used quantitative details such as the spatial distribution and temporal growth behavior of defects to gain conclusive insight into the physical mechanisms that are causing the in-field defects. In this section we extend this analysis to include the defects seen at higher ISO settings.

3.1 Temporal growth of defects

To track the defect growth rate of each individual camera, we need to obtain the actual development date for each defect. To this end, we use information from past images taken by the camera since each image captured is a record of the state of the sensor at the capture time. This procedure, which uses a Bayes statistical analysis to identify the presence of a defect, was described in detail in previous papers [2,3]. By searching through the entire image dataset of a given camera, we can extract the time of the first appearance of each defect as shown in Figure 4 from the EXIF data tag for the image. In the past, we performed this search using visual inspection of pictures, but this process is very slow and cumbersome when applied to a large collection of data. We later developed an automated defect trace algorithm for estimating the first appearance date of each defect, which o includes the effect of the ISO settings[6].

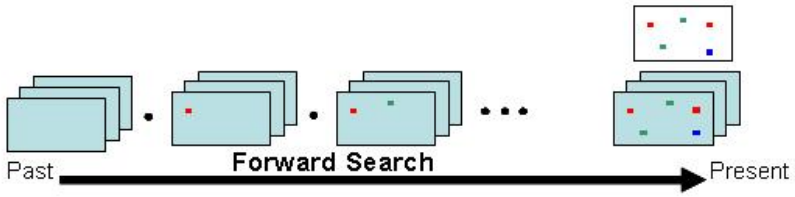

Figure 4: Defect trace algorithm.

We used the algorithm mentioned in the previous section on the image dataset of six cameras with age ranging between 2 and 6 years. The average size of the sensor in these cameras is 23×16mm and the average pixel size is 6.5×6.5µm. With our improved calibration procedure, more defects were identified at high ISO. The following analysis is based on defects identified at ISO 1600. The six cameras we analyzed had a total of 65 defects.

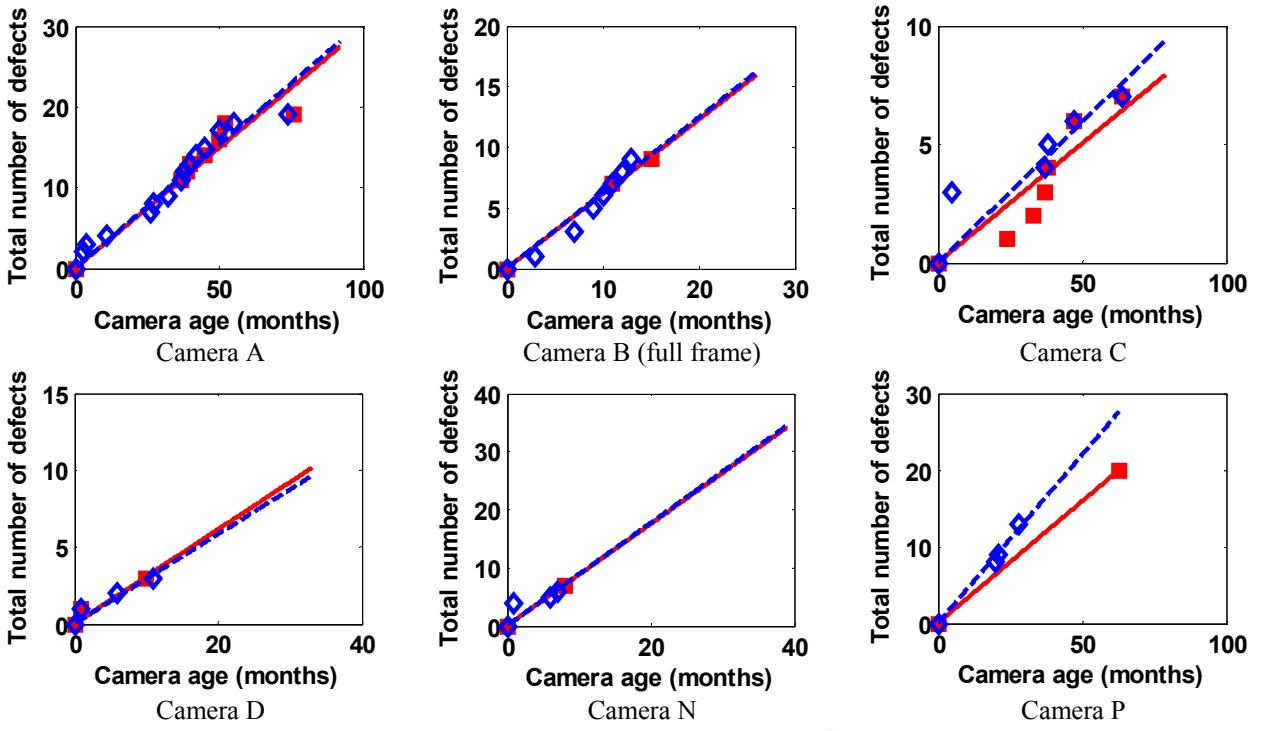

Figure 5: Defect growth rate (using the Bayes defect trace algorithm)

To determine the defect growth rate for each camera, we plot the number of identified defects vs. the camera age as shown in Figure 5, and the growth rate is estimated using a linear fit function. With the six cameras we have over 30,000 pictures, therefore it was not feasible to perform visual inspection of each image for testing the accuracy of the automated algorithm results. An alternative solution for testing our results was to utilize the defect count we obtained from manual calibration. For each of the cameras, we performed a dark frame calibration on a yearly basis; the defect count collected from these calibrations can provide an estimate of the growth rate of defects over the sensor lifetime. The growth rate results from both the Bayes defect trace algorithm and the calibration are summarized in Table 3.

In Figure 5 we notice a similar linear increase in the number of defects in these cameras. The linear growth of defects suggests that in-field defects are not likely to be caused by a single traumatic event or material degradation. Material related defects will usually develop a cluster of spatially close defects at around the same time. However, our observed spatial distribution did not indicate any local clustering of defects. In fact, the shortest distance between two defective pixels was 2 pixels. The continuous increase in the number of defects observed in both types of sensors suggests that these sensors are continuously exposed to a similar kind of causal mechanism such as cosmic-ray radiation. This is consistent with similar conclusions in the literature [7,8] .

Table 3. Manual calibration and Bayes detection growth rate comparison at ISO 400

Camera	Defect growth rate (defects/year)		Diff (%)
	Manual Calibration	Bayes Detection	
A	3.57	3.66	2.46
B	7.35	7.47	1.60
C	1.20	1.42	16.54
D	3.68	3.49	5.28
H	0.77	1.09	33.98
N	10.50	10.60	0.99
P	3.81	5.27	32.08

Table 4. Estimated defect rate from calibration result for all tested DSLRs

Camera	Sensor Type	Defect Rate (defects/year)					
		100	200	400	800	1600	3200
A	APS	1.70	2.09	3.57	3.35	3.83	
B	APS	2.18	4.36	7.35	11.38	18.31	20.47
C	APS		0.50	1.15	2.10	3.80	
D	APS	1.20	2.40	3.68	3.86	7.71	
E	APS			1.86	2.14	5.14	
F	APS	1.11	1.56	2.22	2.88	4.85	1.11
G	APS			2.00	2.00	4.00	4.00
H	APS			0.87	1.53	2.62	
I	APS			0.40	1.60	3.20	
J	CCD		2.08	3.86	5.31	9.90	
K	CCD	1.52	2.86	5.69	8.19	13.14	
L	CCD	2.06	3.19	6.70	9.60	12.37	
M	CCD	1.86	3.32	4.98	8.68	14.58	27.88
O	CCD	1.70	2.09	9.82			
N	CCD	2.18	4.36	10.50			
P	CCD		0.50	3.81			
Q	APS	1.20	2.40	0.77			
R	CCD			5.10			
S	CCD			2.53			
U	CCD			4.46			
Average rate (APS):		**1.55**	**2.18**	**2.39**	**3.43**	**5.94**	**9.32**
Average rate (CCD):		**1.82**	**2.86**	**5.75**	**7.94**	**12.50**	**27.88**

Table 5. Sensor size summary

Camera	Sensor Type	Sensor size (mm)	Sensor area (mm^2)	Pixel size (µm)
Full frame DSLR	APS	36.0 × 24.0	864.0	6.26 × 6.26
Average DSLR	APS	23.0 × 15.0	345.0	6.47 × 6.47
Cell phone	APS	5.40 × 4.30	23.11	2.20 × 2.20
PS-A	CCD	7.18 × 5.32	38.20	1.97 × 1.97
PS-B	CCD	5.75 × 4.31	24.80	2.81 × 2.81
PS-C	CCD	5.27 × 3.96	20.90	2.57 × 2.57
PS-D	CCD	6.13 × 4.60	28.20	1.54 × 1.54

Comparing the defect growth rate detected using the continuous manual calibrations, the difference is less than the max error of 22%. The accuracy of the detection using historical photographs depends on the availability of images and the settings used for these images. For a user who does not capture photographs on a regular basis, the number of images used for analysis can be limited and the error can be large. Because the majority of photographs are captured at short exposure times (~1/30s) and ISO setting below 800, low impact defects are barely visible in these images. Recalling the data in Figure 4(a), for images captured at 1/2s exposure time, only ~20% of defects will have $I_{Offset} > 0.2$ at ISO 400. Thus, detection of low impact defects can be challenging, and in the worst case some defects may not be detected.

3.2 Impact of defects in larger area sensors

One of the trends found in new high end DSLRs is the increase in sensor size to a full 36×24mm frame. Camera B from Table 1 is an example of a full frame large area sensor that is 2 years old. Three sets of calibrations had been performed on this camera and the number of defects found in each calibration is summarized in Table 6.

Table 6. Comparison of defect rate/year at various ISO scaled with sensor area.

	100	200	400	800	1600
Mid sized DSLR rate:	1.34	1.64	1.82	2.49	4.45
Expected Fullframe defect rate:	3.70	4.24	4.49	6.20	11.18
Actual Fullframe defect rate:	3.42	4.19	4.65	6.36	11.36

The size of the sensor in Camera B is much larger (864 mm^2) compared to the average midsized APS sensors (~338 mm^2) shown in Table 1, but the size of the pixels remains approximately the same (6-7 µm range). Between the mid size DSLR and the full frame imagers, if the defect rate scaled proportionally with the sensor area, we would expect the defect rate in the full frame sensor to be 2.55x that of the mid-size DSLRs. We were able to measure the defect rate at various ISO levels for these cameras and the comparison of expected and observed defect rate for the full frame sensor is listed in Table 6. We see that the expected rate calculated with the scaling factor resembles closely the observed rate from full frame imagers. Hence this tends to confirm the assumption that if the pixel size is kept nearly constant, the defect rate per year per mm^2 stays nearly constant, independent of the sensor size. Thus, this is a good metric for comparing different sized imagers.

3.3 Impact of small pixels on defect density

The number of pixels in an average commercial digital camera has increased from 3MP in 2002 to 12MP in 2009. In most cameras the size of the sensor remains the same but the size of the pixel is reduced; thus the number of pixels on a sensor increases. In this study we have analyzed cameras from 10 cellphones of the same type and four different types of Point and Shoot (PS) mid priced cameras, all of which have very small sensors. The camera on the cellphones uses a 5MP APS sensor with pixel dimension of 2.2×2.2µm. The size of the pixels in these cellphone cameras is relatively small compared to a DSLR pixel, which is about 6.47×6.47µm. However, the cellphone cameras have very limited camera exposure and ISO control. Hence, we were only able to measure the cellphones at ISO 400. One important fact regarding our cellphones study is that we had 10 identical cameras with the same age and characteristics, which gives more statistical significance to the data.

In addition to cellphone cameras, we have also identified defects from a set of point and shoot cameras. Each of these cameras uses a CCD sensor with area ranging from 20 to 40 mm^2 and pixel size from 1.5 to 2.8µm. The age span of these PS cameras is 1 to 7 years. In PS cameras there is an explicit control for adjusting the ISO setting; thus we were able to calibrate these cameras at various ISO levels. Table 7 shows the count of defects identified from the set of PS cameras. By comparing the number of defects found in the cellphone and PS cameras with the commercial DSLRs, and taking into account the reduced sensor area, we can gain insight into the impact on defects of reduced pixel size.

To identify defects from these cameras, the dark frame calibration procedure used for DSLRs cannot be applied because of the limited controls and functions available on these cameras. In particular, these cellphone cameras do not have explicit exposure control and therefore we cannot conclude whether an identified fault is a hot pixel or a stuck high defect. More importantly, these simple cameras do not provide the raw format function, and therefore all dark images are captured in color mode. Color images generated by digital cameras are often processed with various imaging functions such as demosaicing, noise reduction, white balance, and alike. These imaging functions tend to distort the faulty pixel, causing a single pixel defect to appear as a virtual cluster. To overcome these challenges we had to design a new procedure for calibrating these cameras.

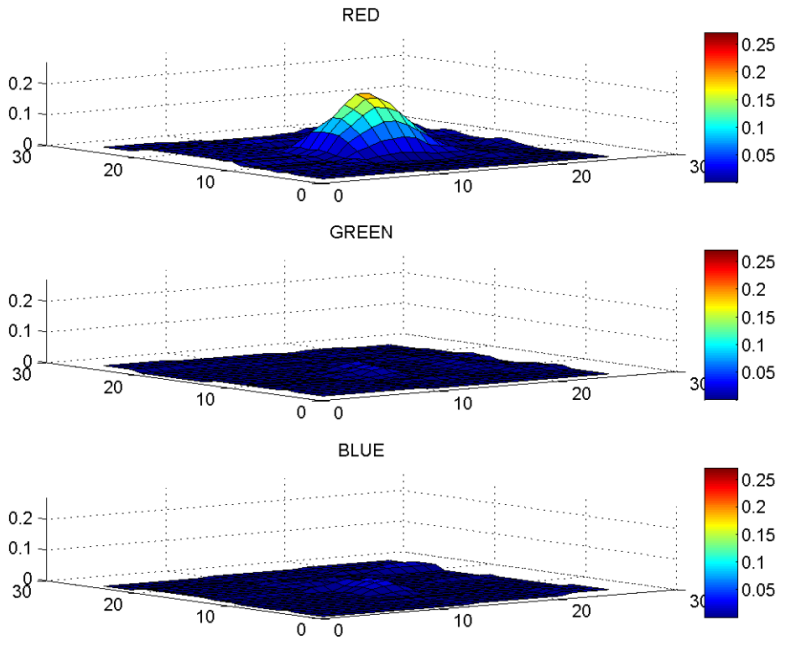

Figure 6. Dark response of a defect identified in a cellphone camera.

First, a hot pixel is most visible in long exposure images; thus we utilize the exposure compensation setting to maximize the exposure time. Next, the ISO setting used in our calibration was ISO 400 as this is the highest level available on this cellphone camera. Finally, to ensure we can capture a dark image, the whole experiment was performed in a dark room condition. To identify defects from the calibration image, we applied a threshold test so that any pixel with an output value greater than the threshold was considered defective. Because defects are identified in color images, demosaicing will cause a single defective pixel to appear as a cluster of defective pixels (Figure 6). Therefore, to achieve the best approximation of the exact defect location, each local cluster was considered as one defective pixel and by finding the peak output within the cluster we determined the exact location of the faulty pixel. Figure 6 shows an example of the local region of the defect identified from our calibration. Plotting the three color planes separately, we can see that this is a red defect and the single peak suggests that the defect is located in a single defective pixel.

Table 7. Accumulated defects from 10 cellphone cameras (ISO400).

Cellphone	2008	2009	2010
Phone A	9	14	18
Phone B	13	15	17
Phone C	8	15	20
Phone D	6	20	24
Phone E	12	21	26
Phone F	14	16	18
Phone G	14	18	20
Phone H	10	19	25
Phone I	14	20	23
Phone J	17	19	22
Cumulative Total:	***117***	***177***	***213***
Average per phone:	***12***	***18***	***21***

To eliminate false detections due to noise, we captured a series of 3 sequential images for each camera and by taking the common result we obtained our final defect set for the cellphone. We have performed three sets of calibrations on the cellphone cameras, the first when the cellphones were first received in 2008 and the other two in 2009 and 2010. The accumulated defect count from the three sets of calibration for the cellphones is summarized in Table 7.

As seen in Table 7, our first calibration identified a total of 117 defects in the 10 cellphone cameras. These cameras are an embedded device in the cellphone, and the mapping of manufacture time defects is not feasible for cost reasons as it is in commercial digital camera. Thus, the defects found in our first calibration may include manufacture time defects plus those developing before the test. Despite the lack of defect mapping from the manufacturer, in our second and third calibration we have identified a cumulative total has doubled to 213 defects. Taking the average number of identified defects per cellphone camera for each calibration, we did a regression fit on the data to get defect rate for each cell in Table 8 and the resulting average defect growth rate for the cellphone cameras to be 3.55 defects/year.

Table 8. Approximated defect rate of cellphone cameras at ISO 400

Cellphone	Offset	Defect Rate (defect/year)
Phone A	8	3.95
Phone B	12	1.97
Phone C	8	4.93
Phone D	14	3.95
Phone E	13	4.93
Phone F	13	1.97
Phone G	15	1.97
Phone H	10	5.92
Phone I	15	2.96
Phone J	14	2.96
	Average rate:	***3.55***

As shown in Table 8, the sensor used in the cellphone is much smaller than the average APS camera from Table 3; the sensor area of the cellphone camera (23.11mm^2) is only 6.8% of the average APS sensors (338 mm^2). In addition, the size of the pixels in a cellphone camera, 2.2×2.2μm, is also much smaller than the pixels in the three APS from Table 3 (6.47×6.47μm). If the number of defects developed in a sensor were proportional to the sensor size, we would expect these cellphone cameras to have a defect rate much lower than the DSLRs, substantially less than 1 defects/year. Thus we would not expect to see a significant increase in defect numbers. If we scale the area of the cellphone sensor to the same sensor size as the DSLRs in Table 3, the 3.55 defects/year would correspond to 52 defects/years in DSLRs. Note that this rate of defects/year is 14 times higher than the observed DSLR rate of 3.7 defects/year. Hence, the cellphone small sensor is showing a much larger defect growth than expected on the basis of DSLRs. The high defect rate in cellphone cameras strongly suggests that the small pixel size may be the reason for a larger number of defects in these sensors.

In a similar set of tests and using the same calibration and detection algorithm, we investigated four Point and Shoot cameras whose parameters are listed in Table 5. In the case of the Point and Shoot cameras, the control of the ISO allowed us to measure each camera over the 100 to 400 ISO range in Table 9. What is notable in Table 10 is that the defect rate per year for the point and shoot cameras is similar to the cellphones and again much higher than would be expected from the rates seen in the DSLR's. The common point in both cellphone and PS cameras is the much smaller pixel size, in the order of 1.6-2.8 microns, compared to the 6-7 micron pixels in the DSLR's. This strongly suggests that the defect rates are significantly higher for smaller pixels.

Table 9: Accumulated defect count of point-and-shoot at various ISO levels

Camera	Sensor Type	Age (year)	Defect count		
			ISO 100	ISO 200	ISO 400
PS-A	CCD	3	7	7	11
PS-B	CCD	6	10	11	27
PS-C	CCD	7	6	7	10
PS-D	CCD	1	0	0	24
Total			***23***	***25***	***72***

Table 10: Approximated defect rate of point-and-shoot at various ISO levels

Camera	Defect Rate (defects/year)		
	ISO 100	ISO 200	ISO 400
PS-A	1.88	1.88	2.95
PS-B	1.58	1.73	4.26
PS-C	0.85	1.00	1.42
PS-D	0.00	0.00	18.88
Average rate:	**1.08**	**1.15**	**6.88**

3.4 Tradeoff between defect rate and sensor size.

In the comparison of the defect rates for the cellphone and point and shoot cameras, with small 1.5-2.8 μm pixels, we have observed that the small pixels have a ~14x higher defect rate than that observed for the DSLR's larger 6-7 μm pixels. In our previous papers, with only the cellphone results, which are a single APS small pixel sensor design, we noted this as an interesting trend. Now with our current results on a wider set of cameras with small pixels there is clear indication that the impact of shrinking pixel size in APS and CCD will be an increase in the defect rates.

We now have sufficient data that makes it possible to explore various relationships between the defect rate and pixel size. Since the small pixel cameras have a much smaller sensor area, it is necessary to scale for that difference. As was noted in Section 4.1, with sensors that have similar pixel sizes the defect rate appears to scale linearly with the sensor area. Thus to remove the sensor area we have plotted the measured defect rate per year per mm^2 (D_a) versus the pixel size (S in microns) for all tested cameras (Table 3, Table 8, and Table 10) for ISO 400, where we have the most camera data points. After observing this data in both linear and semilog plots we found that the curves shown in Figure 9 showed the best relationship between the defect rate and pixel size. This is a log-log plot of defect rate per sensor area vs. pixel size for all the pixel types, and for the APS and CCD sensors directly. Note that all the cellphone measurements were treated as separate data points in this plot. We then did a linear regression fit of Equation (3) which is the power law function of the pixel size as in Equation (4).

$$\log(D_a)=\log(A) + B \log(S) \quad (3)$$

$$D_a=A\, S^B \quad (4)$$

The fit results for all the pixel data is

$$D_a=1.036\, S^{-2.506} \quad (5)$$

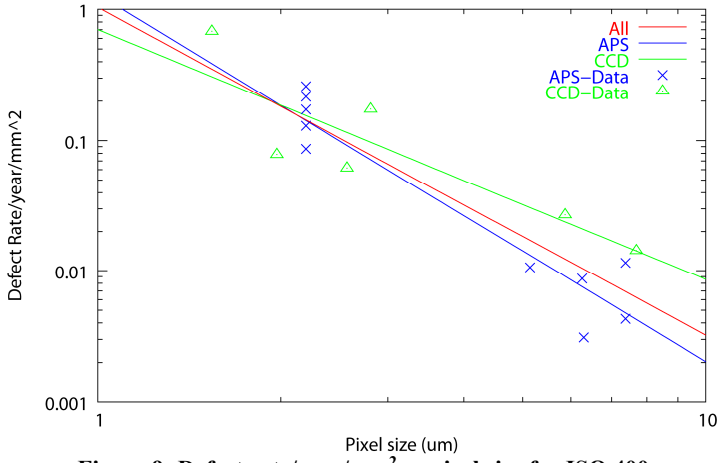

Figure 9: Defect rate/year/mm^2 vs pixel size for ISO 400

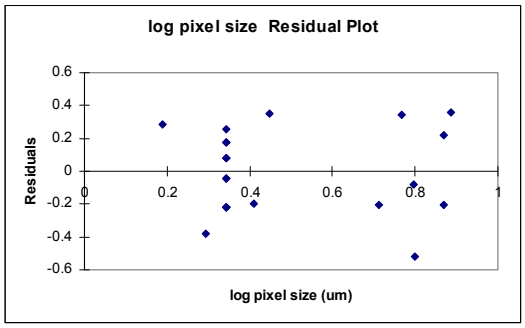

Figure 10: Residuals of Defect rate fit

This fit is very good, having an R^2 =0.83 which gives good confidence in the parameters. The residuals of the fit (Figure 10) are very evenly and randomly distributed with the pixel area, which is a strong indication of the fit formula being correct. This strongly shows that the defect rate per sensor area increases rapidly as the pixel size shrinks. This relationship suggests that the proportionality of defect rate/mm^2 to the pixel area is greater than 1 (one over pixel area would be an S^{-2} relationship).

The question that we then asked is whether this defect rate formula is the same for APS and CCD cameras. Figure 9 shows fits for the combined data set, and for the APS and CCD data separately. In Table 11 and the plots, the separate fits (and parameters) can be observed to bracket the combined fit. However, while the APS appears to increase at a higher power than the CCD, the fit parameters are almost within the statistical error of the fits and so cannot be confirmed at this point. However, these fits only use the best DSLR camera data sets (7 cameras) at this point. A better fit with a larger data set is currently being investigated.

Table 11: Defect rate vs pixel size power law fits for combined, APS and CCD sensors

	A	B
Combined	1.036	-2.506
APS	1.299	-2.806
CCD	0.702	-1.912

Now consider the following possible cause of higher defects with smaller pixels. The average pixel area of DSLRs from Table 3 is ~43.6μm^2. Assuming all pixels have the same efficiency and the same optical system is used, the small pixels from cellphone camera (4.8μm^2) only collect 11% of the light compared to the large pixels. Thus for the small pixel to create similar output, *m* from Equation (1) must increase proportionally. As the scaling factor *m* increases, the impact of a defect, I_{Offset}, as calculated from Equation (2) will increase; therefore a hot pixel which was considered weak in a large pixel is much more visible in a smaller pixel at the same moderate ISO level. This is in agreement with our previous studies [2], which showed that the size of defect causing a hot pixel is very small (<0.07 μm) which is well within the 2.2 μm pixel size. The hot pixel dark current from a given defect remains the same as pixels shrink, but the sensitivity of the pixel to each electron increases; this means that even the weak hot pixels` damage causes a significant effect in smaller pixels. We need to monitor these cellphone and point and shoot cameras over a longer period of time to gain more insight into the cause of the high defect rate. However, it is an important trend to note not only for the cellphones, but as the drive to more pixels in point and shoot and higher end DSLR cameras causes manufacturers to look at smaller pixels, the impact of defects on these small pixels will be a significant drawback on image quality.

4. CONCLUSIONS

In our on-going study of 21 semi-professional cameras, we have observed 243 hot pixels, of which 44% were partially stuck defects. The in-field defects we have observed over the sensor lifetime were permanent and their number increased continuously. In this paper we first looked at the effect of ISO amplification on defects, and found that the majority of defects found in larger area DSLRs are low impact defects, with small dark current. With the increase of amplification required for the high ISO settings, the distinction between background noise and the defects becomes more significant as more low impact defects can be identified. The comparison between DSLRs with different sensor areas but similar pixel sizes (6-7 μm) showed that defect rates appear to scale with the sensor area.

To study the impact of reducing pixel size we also analyzed a set of cellphone cameras and mid sized point and shoot cameras with pixels in the 1.5 to 2.8 μm range. Defect rates were ~14 times that of the DSLR cameras with 6-7 μm. Plotting the defects/year/mm^2 versus pixel size, the best fit was obtained by a power law in pixel size. This suggests that the defect rates/area empirically follow pixel size to the -2.5 power, and approximately inverse to the pixel area.

We conclude that hot pixels will become a much larger issue in the near future. With more high-end DSLRs moving toward larger area sensors and higher ISO ranges, we will be observing more defects which the amplification due to higher ISO and the offset value of many hot pixels will cause to appear over all exposure times. More importantly, with the shrinkage of pixel size, defect rates would rapidly increase. The combination of ISO expansion, sensor area increase and pixel size shrinkage will all significantly increase the rate of hot pixel defect development in cameras and sensors. This suggests important tradeoffs in sensor design parameters for the imager designer.

REFERENCES

[1] J. Dudas, L.M. Wu, C. Jung, G.H. Chapman, Z. Koren, and I. Koren, "Identification of in-field defect development in digital image sensors," *Proc. Electronic Imaging, Digital Photography III*, v6502, 65020Y1-0Y12, San Jose, Jan 2007.

[2] J. Leung, G.H. Chapman, I. Koren, and Z. Koren, "Statistical Identification and Analysis of Defect Development in Digital Imagers," *Proc. SPIE Electronic Imaging, Digital Photography V*, v7250, 742903-1 – 03-12, San Jose, Jan 2009.

[3] J. Leung, G. Chapman, I. Koren, and Z. Koren, "Automatic Detection of In-field Defect Growth in Image Sensors," *Proc. of the 2008 IEEE Intern. Symposium on Defect and Fault Tolerance in VLSI Systems*, 220-228, Boston, MA, Oct. 2008.

[4] J. Leung, G. H. Chapman, I. Koren, Z. Koren, "Characterization of Gain Enhanced In-Field Defects in Digital Imagers," *Proc. of the 2009 Intern. Symposium on Defect and Fault Tolerance in VLSI*, 155-163., Chicago, IL, Oct 2009.

[5] J. Leung, J. Dudas, G. H. Chapman, I. Koren, Z. Koren, "Quantitative Analysis of In-Field Defects in Image Sensor Arrays," *Proc. of the 2007 Intern. Symposium on Defect and Fault Tolerance in VLSI*, 526-534, Rome, Italy, Sept 2007.

[6] J. Leung, G.H. Chapman, Y.H. Choi, R. Thomson, I. Koren, and Z. Koren, "Analyzing the impact of ISO on digital imager defects with an automatic defect trace algorithm", Proc*., Electronic Imaging, Sensors, Cameras, and Systems for Industrial/Scientific Applications XI*, v 7536, 75360F1-0F12, San Jose, Jan. 2010

[7] A.J.P. Theuwissen, "Influence of terrestrial cosmic rays on the reliability of CCD image sensors. Part 1: experiments at room temperature," *IEEE Transactions on Electron Devices*, Vol. 54 (12), 3260-6, 2007.

[8] A.J.P. Theuwissen, "Influence of terrestrial cosmic rays on the reliability of CCD image sensors. Part 2: experiments at elevated temperature," *IEEE Transactions on Electron Devices*, Vol. 55 (9), 2324-8, 2008.